Thermal cycling behaviour of thermal barrier coating systems based on first- and fourth-generation Ni-based superalloys

Cécilie Duhamel[a]*, Marion Chieux[a], Régine Molins[a], Luc Rémy[a], Daniel Monceau[b], Aurélie Vande Put[b] and Jean-Yves Guédou[c]

[a]MINES ParisTech, Centre des Matériaux, UMR CNRS 7633, BP 87-91003 Evry Cedex, France

[b]CIRIMAT, Université de Toulouse, ENSIACET, BP-44362, 31030 Toulouse Cedex 04, France

[c]SNECMA Groupe SAFRAN, Villaroche, 77550 REAU, France

*E-mail: cecilie.duhamel@ensmp.fr

ABSTRACT

This study deals with the cyclic oxidation behaviour of thermal barrier coating systems. The systems consist of an yttria-stabilised zircona ceramic top coat deposited by EB-PVD, a β-(Ni,Pt)Al bond coat and a Ni-based superalloy. Two different superalloys are studied: a first-generation one and a fourth-generation one containing Re, Ru and Hf. The aim of this work is to characterise the microstructural evolution of those systems and to correlate it to their resistance to spallation. Thermal cycling is carried out at 1100°C in laboratory air, with the number of cycles ranging between 10 and 1000. Each cycle consists of a 1 h dwell followed by forced-air cooling for 15 min down to room temperature. Among the main results of this work, it is shown that the MCNG-based system is significantly more resistant to spallation than the AM1-based one. Up to 50 cycles, both systems exhibit similar oxidation rate and phase transformations but major differences are observed after long-term ageing. In particular, a Ru-rich β-phase is formed in the bond coat of the MCNG-based system while the AM1-based one undergoes strong rumpling of the TGO/bond coat interface due to the loss of the thermal barrier coating.

Keywords: thermal cycling behaviour, thermal barrier coating systems, Ni-based superalloys

1. INTRODUCTION

Improvement of the efficiency of high pressure turbines can be obtained by an increase of the gas inlet temperature. Turbine blades of aero-engines are thus subjected to severe environments with high temperatures and high stresses so that high-temperature materials are required. As they offer high mechanical resistance under creep and fatigue conditions, and good resistance to chemical degradation, single-crystal Ni-based superalloys can be used for turbine blades. Since the first-generation superalloys, improvement of the chemistry design has been performed in order to increase their mechanical resistance, in particular their creep properties, and to limit their chemical degradation [1]. Creep-strengthening elements such as rhenium have first been added. However, excessive amounts of these elements lead to the precipitation of topologically closed packed (TCP) phases that are detrimental to the mechanical properties. Ruthenium was introduced a few years ago in the fourth-generation superalloys to reduce the TCP precipitation. In addition, small amounts of reactive elements such as Hf, La and Y in combination with a decrease of the Ti content have

also been shown to be beneficial to the chemical resistance of the superalloys in an oxidising environment [2,3]. Further increase of the gas inlet temperature was also achieved with the development of thermal barrier coating (TBC) systems [4]. TBC systems consist of a ceramic top coat with low thermal conductivity and high permeability to oxygen, covering an alumina-forming metallic bond coat which is resistant to oxidation. Due the high diffusivity of oxygen in the ceramic top coat, a protective thermally grown oxide (TGO) layer of Al_2O_3 forms at the surface of the bond coat during service.

The lifetime of TBC systems is conditioned by the TGO scale adherence which is affected by several factors: (i) growth and thermal stresses in the oxide scale [5]; (ii) phase transformations in the bond coat [6]; (iii) sulfur segregation at the bond coat/TGO interface [7−9]; (iv) cavities at the bond coat/TGO interface [10]; and (v) rumpling [11,12]. Part of those factors depends on the interdiffusion processes occurring between the superalloy and the metallic bond coat at high temperature and consequently on the bond coat and superalloy compositions [6,13,14].

Table 1 Chemical composition (wt.%) of the AM1 and MCNG superalloys

	Ni	Co	Cr	Al	Ti	Ta	Mo	W	Re	Ru	Hf
AM1	64	6.5	7.5	5.3	1.2	8	2	5.5	–	–	–
MCNG	0.4	–	4	6	0.5	5	1	5	4	4	0.1
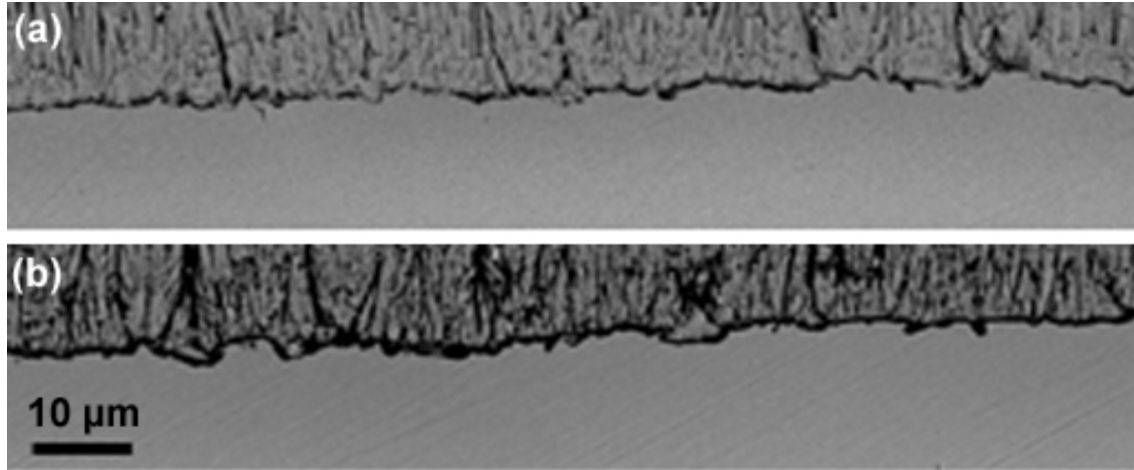
Figure 1 SEM micrographs of cross-sections of the as-coated samples (**a**) AM1-based system, and (**b**) MCNG-based system.

The aim of this work is to study the effect of the super-alloy chemical composition on the spallation resistance of two TBC systems. For this purpose, the cyclic oxidation behaviours of TBC systems with either a first-generation superalloy (AM1) or a fourth-generation superalloy (MCNG) covered by a Pt-modified nickel aluminide bond coat and an yttria-stabilised zirconia top coat are compared.

2. MATERIALS AND METHODS

The samples provided by Snecma are disc-shaped coupons with a diameter of 24 mm, a thickness of 2 mm and chamfered edges. They consist of a β-(Ni,Pt)Al bond coat applied to a Ni-based single-crystal superalloy and covered by the yttria-stabilised zircona (YSZ) top coat deposited by electron-beam physical vapour deposition (EB-PVD). Two superalloys were studied: a first-generation one (AM1) and a fourth-generation one (MCNG) containing Re, Ru and Hf (Table 1). The (Ni,Pt)Al bond coat was obtained by Pt electrodeposition followed by vapour phase aluminising.

Before deposition of the top coat, the surface of the as-prepared samples was grit-blasted. The Ra value of the bond coat surface was measured using a profilometer. For each sample, three 600 μm-long profiles were performed. The Ra value was estimated to 0.7 ± 0.2 μm for the AM1-based systems and 0.5 ± 0.2 μm for the MCNG-based ones. Images of the as-fabricated systems in cross-section are shown in Figure 1.

Thermal cycling was carried out at 1100°C in laboratory air (CIRIMAT facility and standard cycle). Each cycle consisted of a 1 h dwell including heating followed by a forced-air cooling of 15 min down to room temperature. Several ageing times corresponding to 10, 50, 500 and 1000 thermal cycles were tested. The corresponding effective time, defined as the time spent above 97% of 1100°C, is reported in Table 2.

Scanning electron microscopy (SEM) observations of the polished cross-sections of the samples were performed on a field emission gun (FEG) Zeiss Gemini DSM 982 microscope using both the secondary electron imaging mode and the backscattered mode. The profile of the oxide/bond coat

Table 2 Name of the samples and corresponding effective time (h) spent at 1100°C. The effective time is defined as the time spent above 97% of 1100°C

	Name of the sample	Number of cycles	Effective time (h) at 1100°C
AM1/(Ni,Pt)Al/TBC	A10	10	9
	A50	50	45
	A500	500	448
	A1000	1000	896
MCNG/(Ni,Pt)Al/TBC	M10	10	9
	M50	50	45
	M500	500	448
	M1000	1000	896

Table 3 Surface spallation rate (%) after thermal cycling at 1100°C. The sample marked * exhibits 100% of spallation after cutting for sample preparation

|	10 cycles	50 cycles	500 cycles	1000 cycles
AM1/(Ni,Pt)Al/TBC	0	edge	100	100
MCNG/(Ni,Pt)Al/TBC	0	0	edge	edge*

interface was reconstructed by image analysis of low magnification SEM micrographs in order to determine the interface roughness. The interface profile is defined as the line between two different contrasts. A straight line drawn using the method of least squares is used as a reference. This line, which cuts the profile, is drawn in such a way that the total area under the peaks and that under the valleys on each side of this line are equal. The Ra value is calculated as the total area between the profile and the reference line divided by the length of the reference line. Phase transformations and chemical composition in the bond coat were followed respectively by SEM and electron probe microanalysis (EPMA) performed on a CAMECA SX100 apparatus.

3. RESULTS

3.1 Spallation

After thermal cycling at 1100°C, the AM1- and MCNG-based systems exhibited three different levels of spallation (Table 3). No spallation occured on three of the samples: A10, M10 and M50. Three samples show localised spallation close to the edges: A50, M500 and M1000. As this phenomenon is mainly due to a geometrical effect – the ''edge effect'' – leading to stress concentrations, it is not representative of the intrinsic behaviour of the thermal barrier coating system. Therefore, those samples have been assimilated to the ones exhibiting no spallation at all. However, the sample M1000 spalled after cutting for sample preparation. Eventually, the AM1-based samples have totally spalled after 500 and 1000 cycles. Regular visual inspections during thermal cycling revealed that spallation occured at around 200 and 400 cycles, respectively. However, the choice was made to carry out thermal cycling to the duration initially planned. With respect to the previous comments regarding the ''edge effect'', it turned

out that the durability of the MCNG-based systems was strongly improved compared to the AM1-based ones. Indications about the location of spallation are found by several inspections. First, as shown in Figure 2, microcracks exist at, or close to, the oxide/ceramic top coat interface of samples aged for short times (10 and 50 cycles). Such defects were not observed in the as-fabricated systems (Figure 1). The AM1-based systems are more prone to the formation of such defects. SEM observations of the surface of the fully spalled AM1-based samples were also performed. On sample A500, nearly all the surface (>90%) was oxidised but the oxide thickness was not homogeneous [Figure 3(a)–(b)]. XRD analyses coupled with EDS analyses revealed that the oxide consisted mainly of α-Al_2O_3 but other phases such as $NiAl_2O_4$, TiO_2, $AlTaO_4$ and ZrO_2 (tetragonal structure) were also detected [Figures 3(c)–(d) and 4]. Similar phases were observed on sample A1000 (Figure 4). The spinel phase $NiAl_2O_4$ most probably comes from a strong depletion of aluminium in the bond coat, impeding further formation and/or growth of alumina. The titanium and tantalum oxides result from the diffusion of these elements from the superalloy to the surface where they were oxidised. Finally, the presence of ZrO_2 suggests that spallation partially occurred inside the YSZ top coat. ZrO_2 does not form a continuous layer which is consistent with the presence of the microcracks close to but not at the oxide/YSZ interface as previously described. On the contrary, SEM observations of the surface of the MCNG-based sample which spalled after cutting (sample M1000) showed that spallation fully occurs at the oxide/bond coat interface [Figure 5(a)]. Observations of the spalled flakes of the TBC of the MCNG-based system after 1000 cycles revealed the duplex structure of the oxide layer. The internal layer in contact with the bond coat had a columnar structure whereas the external layer in contact with the ceramic top coat had an equiaxed structure with a mean grain size below 1 μm [Figure 5(b)].
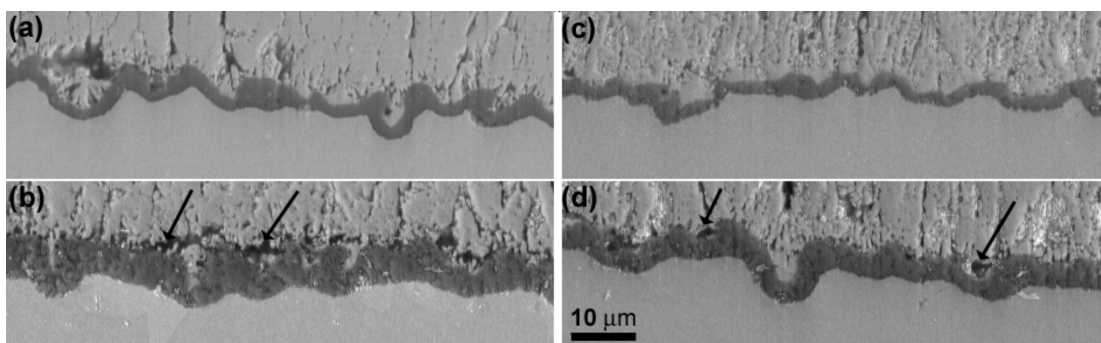
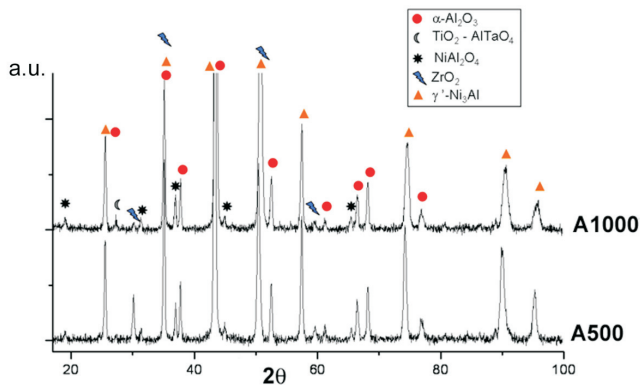**Figure 2** SEM micrographs in SE mode of the oxide layer of the samples: (**a**) A10, (**b**) A50, (**c**) M10 and (**d**) M50. The arrows indicate microcracks.
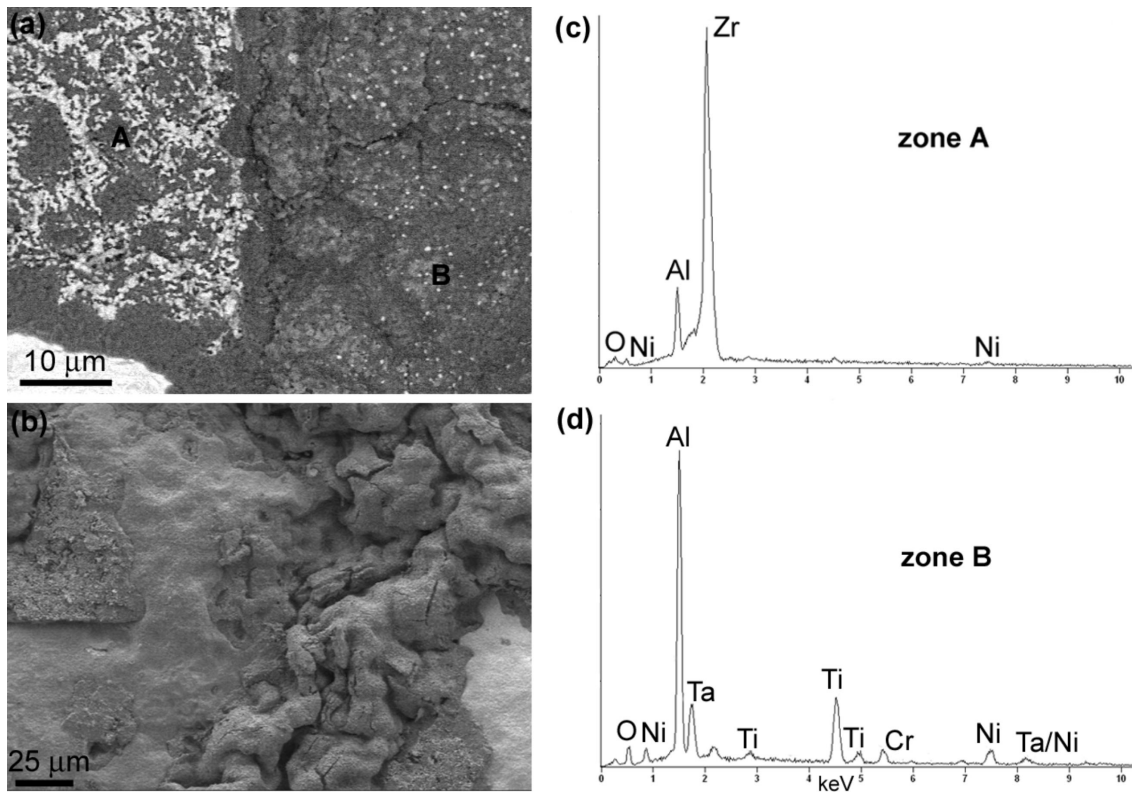
Figure 3 SEM micrograph of the surface of sample A500: (**a**) in backscattered mode, (**b**) in SE mode, (**c**) and (**d**) EDS spectra of zones A and B of SEM image (**a**).

Figure 4 XRD diagrams of the oxide layer of samples A500 and A1000.

3.2 Roughness

The Ra value is used in this study to describe the roughness of the oxide/bond coat interface (Table 4). After 10 and 50 cycles, no significant evolution of the interface roughness was observed for both the AM1- and MCNG-based systems. The Ra values remain in the same range, being slightly higher for the MCNG-based samples. A significant increase of the Ra value is observed after 500 cycles on the MCNG-based sample although no pegs were detected. The interface tends to become smoother after further thermal cycling as suggested by the Ra value after 1000 cycles. After 500 and 1000 cycles, the loss of the ceramic top coat on the AM1-based systems leads to an impressive increase of the Ra value that can reach 6.0 μm. The ceramic layer does not prevent any bond coat surface undulation any more [15].

3.3 Oxidation kinetics

The oxidation kinetics of the two systems was estimated from thickness measurements of the oxide layer obtained from SEM micrographs in cross-section. Although this method is not as precise as thermogravimetric analyses, it enables an estimation of the oxidation rate and a comparison between the two systems. In order to have both sufficient accuracy and representation, several measurements were performed on several high magnification micrographs for each sample. However, after long term ageing, the oxide layer was usually heterogeneous in thickness with differences that can reach a few micrometres. The evolution with time of $(h^2 - h_0^2)$, where h and h_0 refer respectively to the

Table 4 R_a values of the bond coat/oxide interface, estimated by image analysis

|	10 cycles	50 cycles	500 cycles	1000 cycles
AM1/(Ni,Pt)Al/TBC	0.5 ± 0.3	0.7 ± 0.2	6.0 ± 1.0	4.2 ± 1.0
MCNG/(Ni,Pt)Al/TBC	0.8 ± 0.2	1.0 ± 0.2	1.7 ± 0.5	1.0 ± 0.3
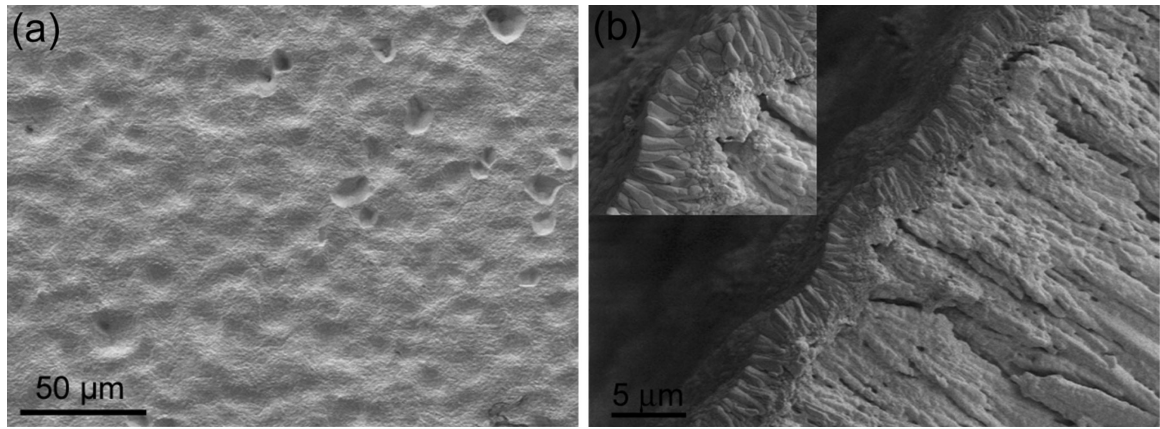
Figure 5 SEM micrograph in SE mode of sample M1000 after spallation: (**a**) surface, and (**b**) spalled flake of the ceramic top coat and oxide layer.

thickness at time t and the initial thickness, is plotted in Figure 6. Because of TBC spallation, no data on the AM1-based system after 500 and 1000 cycles are given. Two domains can be distinguished for the MCNG-based systems with a transition around 50 cycles. As expected, the oxidation kinetics were faster during the first cycles and then decreased for the longer durations. Between 0 and 50 cycles, the AM1- and MCNG-based systems oxidised at a similar rate. The parabolic constants k_p determined from Figure 6 are equal to $2.5 \pm 0.8 \times 10^{-12}\,g^2\,cm^{-4}\,s^{-1}$ for the AM1-based system and $1.9 \pm 0.7 \times 10^{-12}\,g^2\,cm^{-4}\,s^{-1}$ for the MCNG-based system. Between 50 and 1000 cycles, the oxidation kinetics slow down and kp becomes equal to $3.2 \pm 0.7 \times 10^{-12}\,g^2\,cm^{-4}\,s^{-1}$ for the MCNG-based system.

3.4 Phase transformations in the bond coat

In the as-received state, the Pt-modified nickel aluminide bond coat has a duplex structure: the external zone (EZ) is single-phased β-(Ni,Pt)Al while the internal zone (IZ) has a composite structure consisting in a β-(Ni,Pt)Al matrix in
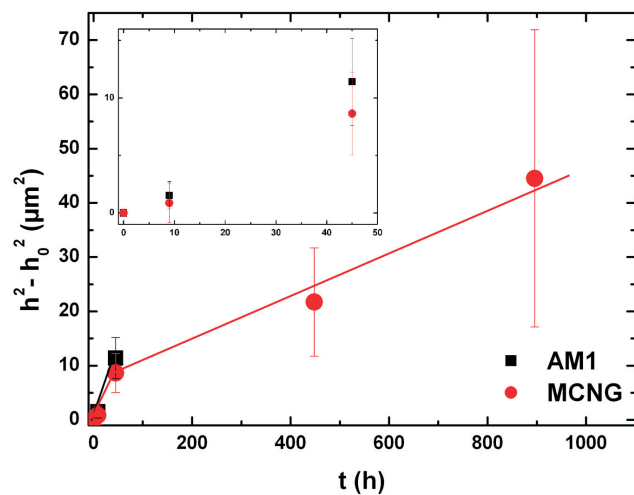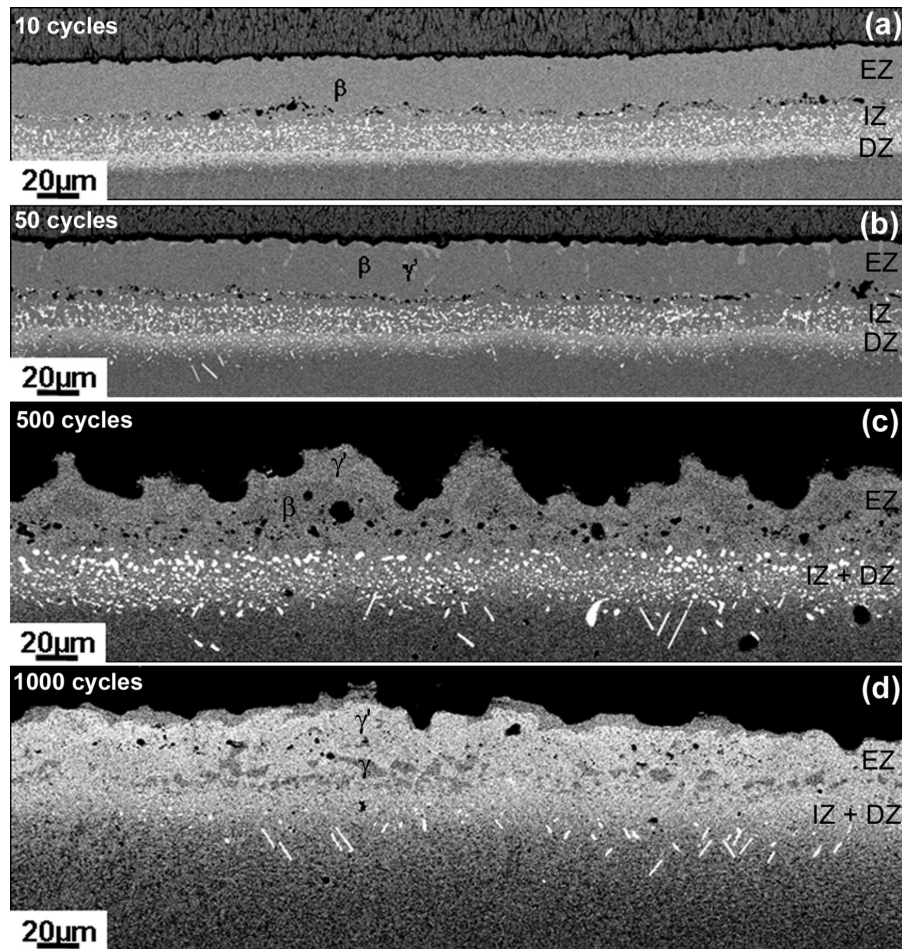

Figure 6 Oxidation kinetics during thermal cycling of the AM1- and MCNG-based systems based on thickness measurements. The insert is a zoom of the plot between 0 and 50 hours.
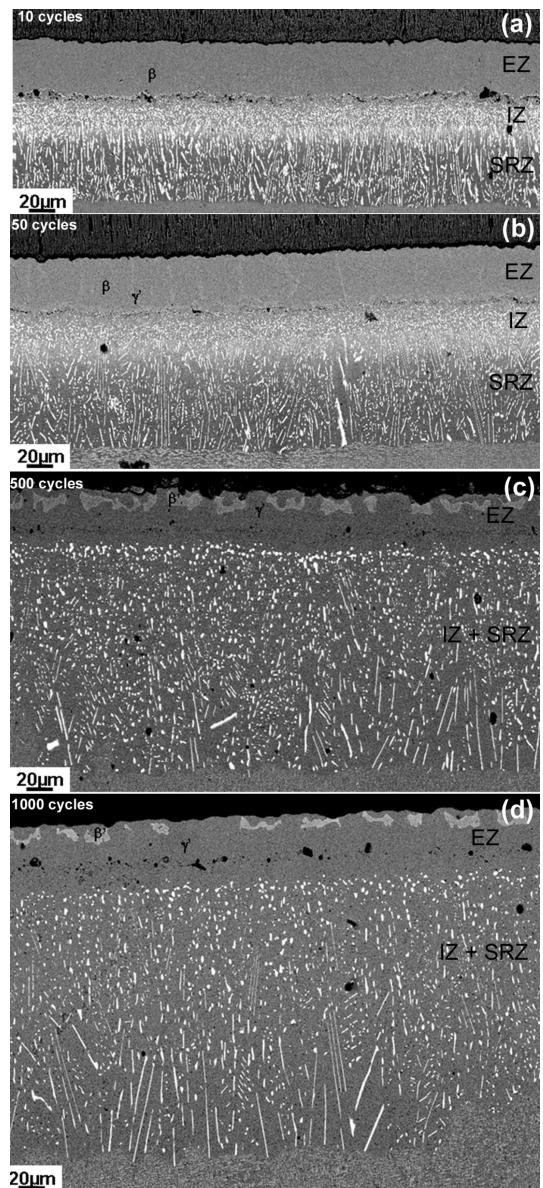
Figure 7 SEM micrographs in BSE mode in cross-sections of the bond coat of the MCNG-based samples: (**a**) M10, (**b**) M50, (**c**) M500, and (**d**) M1000.

Figure 8 SEM micrographs in BSE mode in cross-sections of the bond coat of the AM1-based samples: (**a**) A10, (**b**) A50, (**c**) A500 and (**d**) A1000.

which TCP precipitates are embedded. At the interface with the IZ, destabilisation of the superalloy leads to the formation of a diffusion zone in the AM1-based systems. In the MCNG-based ones, this layer is thicker and is called secondary reaction zone (SRZ) [16,17]. In both cases, the microstructure consists of TCP precipitates embedded in a γ'-Ni$_3$Al matrix. After 10 cycles, no phase transformation was observed by SEM either in the external zone (EZ) or in the internal zone (IZ) of both systems [Figures 7 and 8(a)]. However, the chemical composition of the external zone of bond coat had slightly changed as revealed by WDS analyses (Figure 9). Due to the interdiffusion phenomena between the bond coat and the superalloy, depletion of aluminium associated with enrichment of nickel and to a minor extent of chromium in the EZ of both systems can be seen. In addition, ruthenium coming from the superalloy is detected in the EZ of the MCNG-based system. After 50 cycles, the transformation of the β-phase into the γ'-phase (Ni$_3$Al) was initiated in both systems [Figures 7 and 8(b)]. The phase transformation starts at the grain boundaries, at the oxide/alloy interface and at the EZ/IZ interface. The deple-tion of aluminium carries on in the EZ where the aluminium content reaches 32–33 at.%. After 500 and 1000 cycles, the EZ of the bond coat consisted mainly of the γ'-phase in the MCNG-based systems [Figure 7(c) and (d)]. The γ'-phase is located at the oxide/bond coat interface and at the EZ/IZ

interface. The EZ was considerably enriched in nickel and depleted in aluminium. Significant amounts of chromium and ruthenium were also detected. As shown by chemical analyses of each of the two phases (Table 5), the ruthenium was nearly exclusively dissolved into the β-phase where its content reaches 13.4 at.% after 500 cycles and 20 at.% after
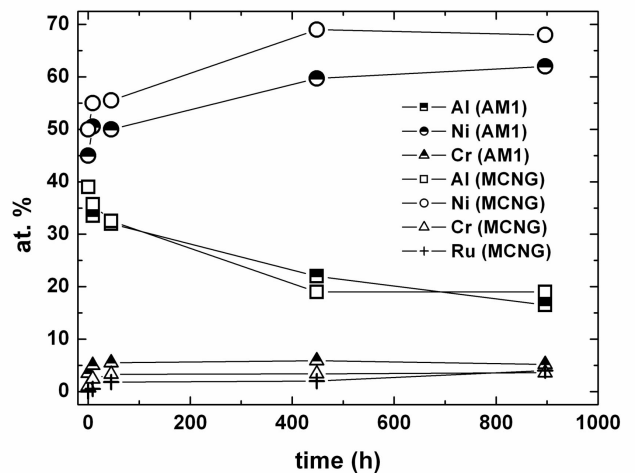
Figure 9 Evolution with time of the Al, Ni, Cr and Ru contents of the external zone of the bond coat for both systems.

Table 5 Chemical composition (at.%) determined by WDS of the β- and γ′-phases in the external zone of the samples M500 and M1000

		Al	Ni	Pt	Cr	Ti	Ta	W	Mo	Re	Ru
M500	β	33	44	3.4	5.5	0.4	0.2	0.3	0.1	0.1	13.4
M500	γ′	19.2	71.7	2.2	3.5	0.5	1.2	1	0.4	0.2	1.6
M1000	β	35	32.6	3.1	5.7	0.7	0.5	0.4	0.1	0.1	20
M1000	γ′	18.6	70	1.8	3.5	0.5	1.3	1.1	0.4	0.3	1.9

1000 cycles. In addition, in the IZ, the β-phase was fully transformed into the γ′-phase and no distinction can be made between the IZ and the SRZ. The total thickness of these two zones drastically increases up to 159 μm after 500 cycles and 186 μm after 1000 cycles (Figure 10). The TCP precipitates in the SRZ grow towards the superalloy and perpendicularly to the interface whereas a layer free of TCP precipitates appears below the alumina particles at the EZ/IZ. For the AM1-based systems after 500 and 1000 cycles, the loss of the thermal barrier coating leads to a strong rumpling which increases the length of TGO/bond coat interface and thus the surface to be oxidised. The aluminium depletion in the external zone was enhanced and a high degree of transformation of the β-phase into the γ′-phase was observed after 500 cycles [Figure 8(c)]. The β-phase in the IZ is fully transformed into the γ′-phase and the IZ can no longer be distinguished from the diffusion zone (DZ). After 1000 cycles, the aluminium content in the EZ was low (16.5 at.%). No more β-phase was observed and the γ′-phase had begun to transform into the γ-phase (Figure 8(d)).

4. DISCUSSION

4.1 Effect of the superalloy composition

The objective of this work is to study the effect of the superalloy composition on the durability and degradation of thermal barrier coating systems during thermal cycling. The two superalloys studied differ by the addition of rhenium, ruthenium and hafnium in the fourth-generation superalloy (MCNG). The durability of the systems is evaluated through

Figure 10 Evolution with time of the thickness of (i) the external zone and (ii) the internal zone added to the diffusion zone/SRZ for the AM1-based and MCNG-based systems.

their resistance to spallation after a given number of thermal cycles. According to the results described previously, the MCNG-based system is more resistant to spallation than the AM1-based system. Indeed, the former can sustain at least 1000 cycles while the latter fails between 200 and 400 cycles. The origin of this better resistance to spallation is difficult to explain. Several factors affecting the spallation of the TBC systems have been reported in the literature [4] such as the oxidation kinetics, the nucleation and growth of cavities at the oxide/bond coat interface, phase transformations in the bond coat, rumpling, *etc*.

The oxidation kinetics of the two systems are in the same range, at least up to 50 cycles, and are consistent with the literature [6,18,19]. However, the parabolic constant k_p is slightly lower for the MCNG-based system than for the AM1-based one. The MCNG superalloy contains a reactive element (Hf) that can segregate to the oxide/bond coat interface and thus slow down the oxidation rate [20]. Such a segregation of hafnium at the oxide/alloy interface and in the grain boundaries of the oxide has already been evidenced [21]. For a higher number of cycles, the oxidation rate of the MCNG-based system decreases, probably because of microstructural evolution in the TGO.

Due to oxidation and interdiffusion between the superalloy and the bond coat, the chemical composition of the bond coat evolves during thermal cycling. For both systems, the external zone becomes more and more depleted in aluminium and enriched in nickel. In addition, elements coming from the superalloy are detected in the bond coat. According to the equilibrium phase diagram, the aluminium depletion leads to the transformation of the β-phase into the γ′-phase [22]. After 10 and 50 cycles, the magnitude and the nature of the phase transformations in the bond coat are similar in both systems as well as the nickel and aluminium contents in the EZ. After 500 and 1000 cycles, the comparison between the two systems becomes difficult as the loss of the ceramic top coat and the strong rumpling on the AM1-based ones may have a direct influence on the microstructural evolutions of the bond coat. However, two main differences can be pointed out, independently of any spallation effect. Firstly, due to the diffusion of ruthenium in the bond coat of the MCNG-based systems, the transformation of the β-phase (Ni,Pt)Al into a Ru-rich β-phase (Ni,Pt,Ru)Al is observed. Secondly, the SRZ in the MCNG-based systems is at least three times thicker than the diffusion zone in the AM1-based systems. This enhanced interdiffusion phenomenon between the bond coat and the superalloy in the MCNG-based systems leads to an accelerated depletion of the aluminium reservoir constituted by the nickel aluminide bond coat. In addition, due to the brittle TCP phases, the SRZ exhibits degraded mechanical resistance compared to the initial superalloy [19].
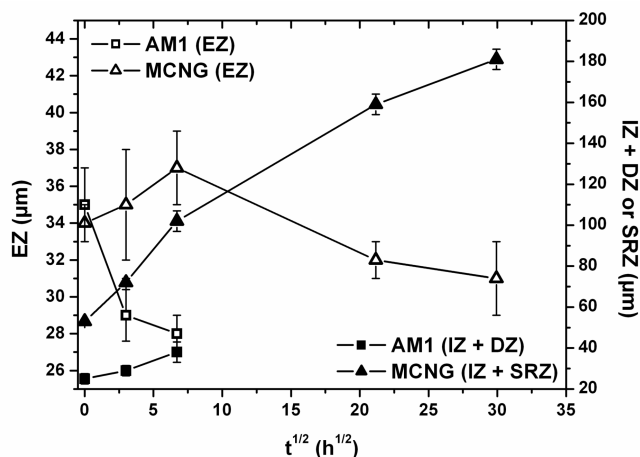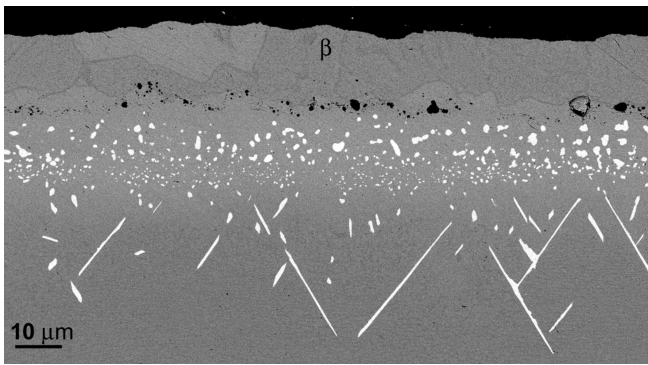
Figure 11 SEM micrograph in BSE mode in cross-section of the bond coat of a AM1/(Ni,Pt)Al sample after isothermal oxidation at 1100°C for 1000 h.

Another consequence of interdiffusion between the super-alloy and the bond coat is the presence of titanium in the TGO. Titanium oxide has been detected in the TGO of the AM1-based systems that have spalled. Above a certain amount, titanium has been reported to be detrimental to the spallation resistance of the systems [6,23]. As AM1 contains a higher titanium content than MCNG (1.2 wt.% *versus* 0.5 wt.%), this is another possible explanation to account for the better resistance to spallation of the MCNG-based systems.

4.2 Degradation mode

Among all the samples tested, two of them spalled sponta-neously during thermal cycling (A500 and A1000) whereas one spalled a few days after the end of thermal cycling (M1000). For the latter, spallation occurs at the TGO/bond coat interface and is attributed to the exposure of the sample to air humidity, also called Desktop Spallation (DTS) [24]. Determining where spontaneous spallation occurs on the AM1-based systems is more difficult. On the one hand, the presence of ZrO_2 nodules at the surface of the spalled samples suggests that spallation occurs partly at the oxide/top coat interface. This is also consistent with the pores and microcracks observed in cross-section close to this interface. On the other hand, comparison with isothermal oxidation of an AM1/(Ni,Pt)Al system at 1100°C for 1000 h shows that, after isothermal treatment: (i) the degree of phase transformations is lower (Figure 11), and (ii) α-Al_2O_3 is the only oxide detected [25]. One possible scenario to account for these observations is that spallation also occurs at the oxide/bond coat interface. Reoxidation of the spalled areas leads to the formation of transient alumina that further transform into α-Al_2O_3. This process of spallation/reoxida-tion most probably occurs periodically during thermal cycling, explaining the heterogeneous thickness of the oxide layer after 500 or 1000 cycles. Due to the higher growth kinetics of transient alumina and to a strong rumpling which increases the total surface of the bond coat, depletion of aluminium in the external zone is enhanced until reaching the critical content of aluminium for the formation of Al_2O_3. New oxides such as $NiAl_2O_4$ then form. In the bond coat,

aluminium depletion is evidenced by the transformation of the γ'-phase into the γ-phase.

Another feature associated with TBC systems degradation is the bond-coat rumpling, which is manifested by periodic undulations of the oxide/bond coat interface due to plastic deformation of the bond coat [11]. Although the existence of such undulations has been pointed out by SEM observations in cross-section, their evolution with cycling (for the samples which do not spall) is low as shown by the Ra values. The extent of the rumpling phenomenon strongly increases with: (i) the absence of the ceramic top coat: on the AM1-based systems, the loss of the thermal barrier coating induces a high increase in the Ra values; and (ii) the cyclic nature of the oxidation treatment. The Ra values of the oxide/bond coat interface of the AM1/(Ni,Pt)Al system oxidised isother-mally [25] is around 2 μm, *i.e.* between twice and three times lower than the Ra values obtained after thermal cycling. A similar trend was observed by Tolpygo *et al.* [26].

5. CONCLUSION

The effect of the superalloy composition on the spallation resistance of TBC systems has been studied. Two super-alloys were compared: a first-generation one (AM1) and a fourth-generation one (MCNG). It emerges from this study that:

- The MCNG-based system is more resistant to spallation than the AM1-based one. The MCNG-based system can sustain at least 1000 1 h-cycles at 1100°C (or 500 1 h-cycles when including the DTS) while the AM1-based one spontaneously spalls between 50 and 500 cycles.
- Up to 50 cycles, the oxidation kinetics of both systems stand in the same range. A decrease in the oxidation rate of the MCNG-based systems is observed after 50 cycles.
- Up to 50 cycles, similar phase transformations are observed. At 500 and 1000 cycles, the β-phase in the bond coat of the MCNG-based systems is considerably enriched in ruthenium coming from the superalloy. In addition, the SRZ significantly extends.
- The loss of the ceramic top coat in the AM1-based systems induces significant rumpling of the TGO/bond coat interface, which leads to enhanced oxidation and subsequent aluminium depletion within the bond coat.

REFERENCES

[1] Caron P. and Khan, T. (1999) Evolution of Ni-based super-alloys for single crystal blade application. *Aerospace Sci. Technol.*, **3**(8), 513–523.

[2] Diologent, F., Caron, P., Jacques, A. and Bastie, P. (2002) Creep behavior at 1050°C of a new generation single crystal superalloy. In: Mishra, R.S., Earthman, J.C. and Raj, S.V. (eds), *Creep deformation: fundamentals and applications*, pp. 361–370.

[3] Reed, R.C. (2008) *The superalloys: fundamentals and appli-cations*. Cambridge University Press.

[4] Gleeson, B. (2006) Thermal barrier coatings for aeroengine applications. *J. Prop. Power*, **22**(2), 375–383.

[5] Evans, A.G., He, M.Y. and Hutchinson, J.W. (2001) Mechanics-based scaling laws for the durability of thermal barrier coatings. *Prog. Mater. Sci.*, **46**, 248–271.

[6] Vialas, N. and Monceau, D. (2006) Substrate effect on the high-temperature oxidation behavior of a Pt-modified aluminide coating. Part I: Influence of the initial chemical composition of the coating surface. *Oxid. Met.*, **66**(3/4), 155–189.

[7] Hou, P.Y. and Stringer, J. (1992) Oxide scale adhesion and impurity segregation at the scale/metal interface. *Oxid. Met.*, **38**(5/6), 323–345.

[8] Molins, R., Rouzou, I., Rémy, L., Le Biavant-Guerrier, K. and Jomard, F. (2005) Study of sulfur distribution in a NiPtAl bondcoat. *Mater. High Temp.*, **22**(3–4), 359–366.

[9] Molins, R., Rouzou, I. and Hou, P.Y. (2007) A TEM study of sulfur distribution in oxidised Ni40Al and its effect on oxide growth and adherence. *Mater. Sci. Eng. A*, **454–455**, 80–88.

[10] Brumm, M.W. and Grabke, H.J. (1993) Oxidation behaviour of NiAl. II: Cavity formation beneath the oxide scale on NiAl of different stoichiometries. *Corros. Sci.*, **34**, 547.

[11] Evans, A.G., Mumm, D.R., Hutchinson, J.W., Meier, G.H. and Pettit, F.S. (2001) Mechanisms controlling the durability of thermal barrier coatings. *Prog. Mater. Sci.*, **46**(5), 505.

[12] Tolpygo, V.K. and Clarke, D.R. (2004) On the rumpling mechanism in nickel-aluminide coatings - Part I: an experimental assessment. *Acta Mater.*, **52**, 5115–5127.

[13] Pint, B.A., Haynes, J.A., More, K.L., Wright, I.G. and Leyens, C. (2000) Compositional effects on aluminide oxidation performance: Objectives for improved bond coats. In: Pollock, T.M., Kissinger, R.D., Bowman, R.R., Green, K.A., McLean, M., Olson, S.L. and Schirra, J.J. (eds), *Superalloys 2000*, pp. 629–638.

[14] Pint, B.A., Wright, I.G., Lee, W.Y., Zhang, Y., Prüssner, K. and Alexander, K.B. (1998) Substrate and bond coat compositions: factors affecting alumina scale adhesion. *Mater. Sci. Eng., A*, **245**, 201.

[15] Tolpygo, V.K. and Clarke, D.R. (2000) Surface rumpling of a (Ni,Pt)Al bond coat induced by cyclic oxidation, *Acta Mater.*, **48**, 3283–3293.

[16] Matsuoka, Y., Aoki, Y., Matsumoto, M., Satou, A., Suzuki, T., Chikugo, K. and Murakami, K. (2004) The formation of SRZ on a fourth generation single crystal superalloy applied with aluminide coating. In: Green, K.A., Pollock, T.M., Harada, H., Howson, T.E., Reed, R., Shirra, J.J. and Walston, S. (eds), *Superalloys 2004*, pp. 637–642.

[17] Walston, S., Schaeffer, J.C. and Murphy, W.H. (1996) A new type of microstructural instability in superalloys–SRZ. In: Kissinger, R.D. (ed.), *Superalloys 1996*, pp. 9–18.

[18] Brumm, M.W. and Grabke, H.J. (1992) The oxidation behavior of NiAl. I. Phase transformation in the alumina scale during oxidation of NiAl and NiAl-Cr alloys. *Corros. Sci.*, **33**, 1677–1690.

[19] Cavaletti, E., Naveos, S., Mercier, S., Josso, P., Bacos, M.P. and Monceau, D. (2009) Ni-W diffusion barrier: its influence on the oxidation behaviour of a *β*-(Ni,Pt)Al coated fourth generation nickel-base superalloy. *Surf. Coat. Technol.*, **204**, 761–765.

[20] Pint, B.A. (1996) Experimental Observations in support of the dynamic-segregation theory to explain the reactive-element effect. *Oxid. Met.*, **45**(1/2), 1–37.

[21] Pint, B.A. and More, K.L. (2009) Characterisation of alumina interfaces in TBC systems. *J. Mater. Sci.*, **44**, 1676–1686.

[22] Hayashi, S., Ford, S., Young, D., Sordelet, D., Besser, M. and Gleeson, B. (2005) α-NiPt(Al) and phase equilibria in the Ni-Al-Pt system at 1150°C. *Acta Mater.*, **53**, 3319–3328.

[23] Tawancy, H.M., Mohamed, A.I. and Abbas, N.M. (2003) Effect of superalloy substrate composition on the performance of a thermal barrier coating system. *J. Mater. Sci.*, **38**, 3797–3807.

[24] Smialek, J.L. (2002) Scale adhesion, sulfur content, and TBC failure on single crystal superalloys. *Ceram. Eng. Sci. Proc.*, **23**(4), 485–495.

[25] Chieux, M., Molins, R., Remy, L., Duhamel, C. and Cadoret, Y. (2009) Adhesion of thermal barrier coatings systems after long term oxidation: influence of preoxidation temperature and surface state of the bond coat. *Mater. High Temp.*, **26**, 187–194.

[26] Tolpygo, V.K. and Clarke, D.R. (2007) Temperature and cycle-time dependence of rumpling in platinum-modified diffusion aluminide coatings, *Scripta Mater.*, **57**, 563–566.